

# Carbon Fiber-Mediated Electrospinning Scaffolds Can Conduct Electricity for Repairing Defective Tendon

Xiao Yu,<sup>†</sup> Genbin Wu,<sup>†</sup> Pengfei Cai, Yangfan Ding, Jie Cui, Jinglei Wu, Yihong Shen, Jiahui Song, Zhengchao Yuan, Mohamed EL-Newehy, Meera Moydeen Abdulhameed, Huifang Chen, Xiumei Mo,\* Binbin Sun,\* and Yinxian Yu\*



Cite This: <https://doi.org/10.1021/acsami.4c12245>



Read Online

ACCESS |



Metrics & More

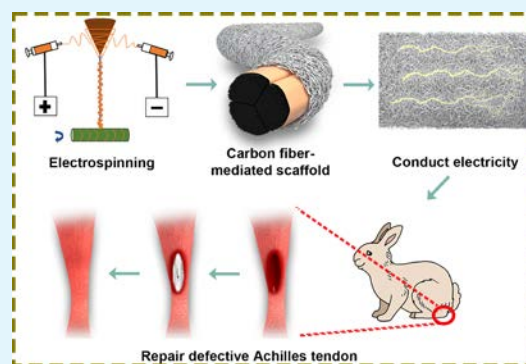


Article Recommendations



Supporting Information

**ABSTRACT:** Partial or complete rupture of the tendon can damage the collagen structure, resulting in the disruption of the electrical signal pathway. It is a great challenge to reconstruct the original electrical signal pathway of the tendon and promote the regeneration and functional recovery of defective tendon. In this study, carbon fiber-mediated electrospinning scaffolds were fabricated by wrapping conductive, high-strength, loose single-bundle carbon fibers with nanofiber membranes. Due to the presence of nanofiber membranes, the maximum tensile force of the scaffolds was 2.4 times higher than that of carbon fibers, while providing excellent temporal and spatial prerequisites for tenocytes to adapt to electrical stimulation to accelerate proliferation and expression. The diameter of the carbon fiber monofilaments used in this study was  $5.07 \pm 1.20 \mu\text{m}$ , which matched the diameter of tendon collagen, allowing for quickly establishing the connection between the tendon tissue and the scaffold, and better promoting the recovery of the electrical signal pathway. In a rabbit Achilles tendon defect repair model, the carbon fiber-mediated electrospinning scaffold was almost filled with collagen fibers compared to a nonconductive polyethylene glycol terephthalate scaffold. Transcriptome sequencing revealed that fibromodulin and tenomodulin expression were upregulated, and their related proteoglycans and glycosaminoglycan binding proteins pathways were enhanced, which could regulate the TGF- $\beta$  signaling pathway and optimize the extracellular matrix assembly, thus promoting tendon repair. Therefore, the scaffold in this study makes up for the shortage of conductive scaffolds for repairing tendon defects, revealing the potential impact of conductivity on the signaling pathway of tendon repair and providing a new approach for future clinical studies.



**KEYWORDS:** carbon fiber, electrospinning, conductive, collagen, repair defective tendon

## 1. INTRODUCTION

Tendons, the connective tissue that connects muscles and bones, are an important part of the musculoskeletal system for storing and transferring energy during movement.<sup>1,2</sup> Tendons are composed of bundles of collagen fibers arranged along their longitudinal axis. The regulation of collagen fibers within tendons is complex: involving the formation of tropocollagen, collagen fibrils, collagen fibers, and fascicles. Finally, the tendon matrix is composed of fascicles. The diameter of collagen fibers is 1–20  $\mu\text{m}$ .<sup>3,4</sup> However, partial or complete rupture of tendons due to accidents or excessive exercise can cause changes in collagen homotypic expression and tertiary structure, disrupting collagen alignment, leading to loss of function, and reducing mobility.<sup>5,6</sup>

It is notable that tendons exhibit piezoelectric characteristics, which can convert mechanical energy into electrical energy, and the piezoelectric behavior is related to collagen.<sup>7,8</sup> The endogenous electric field is the basis for the conduction of bioelectric signals and is a priority signal for the regeneration of damaged tissues.<sup>9</sup> It has been shown that bioelectric signals

generated during physiological exercise can activate tendon-specific regenerative pathways.<sup>10,11</sup> Therefore, it is feasible to accelerate the migration of tenocytes by controlling the bioelectricity within tendons, thereby promoting tendon repair.<sup>12</sup> It is well-known that electrical stimulation (ES) promotes directional cell migration and alignment, affects cell proliferation and differentiation, influences cell membrane contractility, permeability and energy transfer, and also regulates pH changes.<sup>8,13–15</sup> Therefore, ES can guide the development and regeneration of many tissues.<sup>16</sup> For example, Carla et al.<sup>17</sup> confirmed that micro-ES accelerated cartilage repair at non-articular sites in animals.

**Received:** July 22, 2024

**Revised:** September 5, 2024

**Accepted:** September 10, 2024

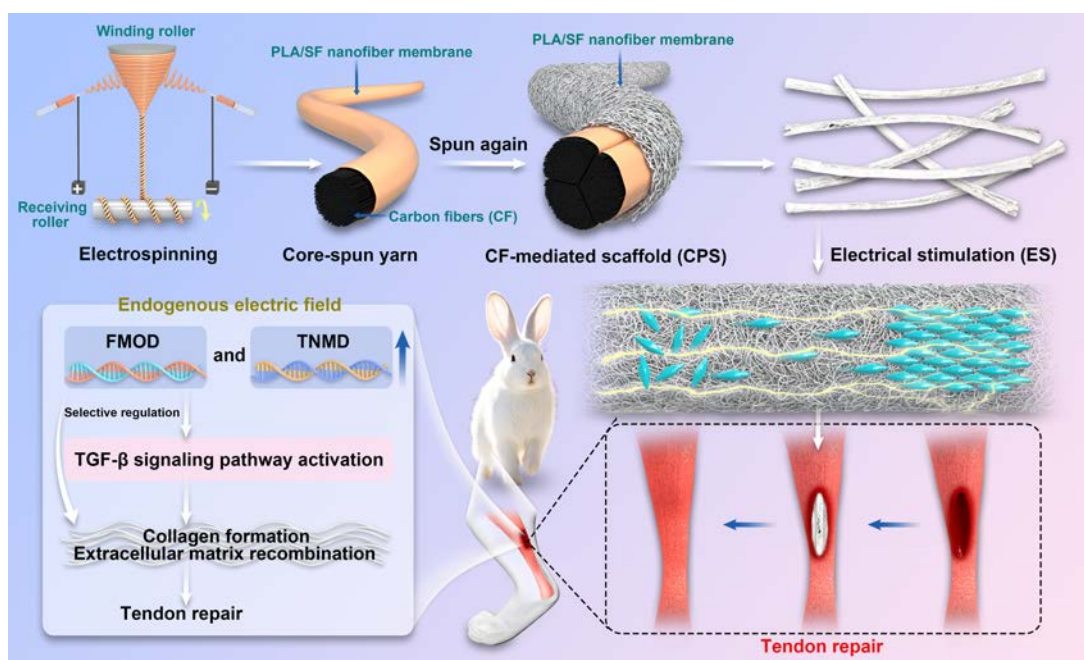


**Figure 1.** Schematic illustration of the preparation and application of the CPS. First, the core-spun yarn was obtained by electrospinning, in which the reinforcing core was CF and the nanofiber membrane was PLA/SF. Second, the three bundles of core-spun yarn were combined and spun again to obtain a thicker CF-mediated scaffold. Then, tenocytes were seeded on CPS and given ES *in vitro*, which could influence tenocytes migration, proliferation, and alignment. Finally, the CPS was implanted into the Achilles tendon defect area of rabbits, and the CPS could promote tendon repair under the action of endogenous electric field in the organism.

The complexity of the surgery and external ES can lead to frequent postoperative risks. Therefore, it is necessary to utilize implantable biomaterials that can spontaneously conduct electricity under the influence of bioelectric signals within the organism to facilitate tissue repair.<sup>18</sup> The inherent conductivity of conductive biomaterials allows the transmission of ion signals in the cell process, which can guide the directional arrangement of cells and promote cell differentiation in various tissue types. Conductive biomaterials have been widely utilized in tissue engineering, including carbon nanotubes, carbon nanoyarns, and mixed biomaterials of graphene and metal particles (such as gold nanoparticles).<sup>19</sup>

Ideally, engineering scaffolds for tendon repair and regeneration require sufficient strength to withstand large cyclic loads, resist long-term creep deformation, and allow for the effective transfer of nutrients and wastes.<sup>20</sup> According to the initial study, carbon fibers (CF) exhibited minimal foreign body sensation and could be infiltrated by new collagen tissue.<sup>21</sup> Wang et al.<sup>22</sup> have developed layered spiral carbon nanotube fibers as ligament substitutes, which were biocompatible and had high tensile strength. The carbon nanotube fibers bonded well with natural bone and were sturdy enough to allow animals to run and jump normally after 13 weeks of implantation in rabbits and sheep. Howard et al.<sup>23</sup> used CF to repair ruptured Achilles tendons in humans, and the results showed that the Achilles tendons healed well in most patients. The above indicates that CF has conductivity, biocompatibility, and good mechanical properties, which has potential value as a substitute scaffold for tendons. However, each bundle of CF is made up of multiple monofilaments, which are extremely loose. Electrospinning is a technology that can be used to make nanofibers in a variety of forms.<sup>24,25</sup> Interestingly, the CF can be wrapped and used as a stable independent scaffold through electrospinning. Poly(lactic acid) (PLA) is a

biocompatible and biodegradable medical polymer that exhibits piezoelectric properties after appropriate treatment to create safer implants, such as electrospun poly(L-lactic acid) membranes produced by spinning a roller at high speed for cartilage regeneration.<sup>26,27</sup> Silk fibroin (SF) has good biocompatibility and has been used to mix with various conductive materials to create SF-based conductive scaffolds for tissue repair.<sup>28</sup>

In this study, CF was electrospun to obtain a bundle of core-spun yarn, in which the shell layer was nanofiber membranes of PLA/SF and the core layer was CF. Then multiple core-spun yarns were combined and spun again to obtain a three-dimensional CF-mediated electrospinning scaffold that could repair a defective tendon. The oriented CF monofilaments with a diameter of  $5.07 \pm 1.20 \mu\text{m}$  were used to simulate collagen fibers in the tendon. The nanofiber membranes mimicked the connective tissue that wraps around collagen fibers in the tendon. In this way, we hope that conductive CF can replace the missing collagen fibers at the site of tendon defect, and generate electrical signals under the action of the endogenous electric field in the organism, thereby accelerating cell migration, proliferation, differentiation and expression, and finally promoting tendon repair. In this study, non-conductive polyethylene glycol terephthalate yarn and CF were selected as controls to verify whether the CF-mediated electrospinning scaffolds can promote tendon repair.

## 2. EXPERIMENTS AND METHODS

**2.1. Materials.** The polyethylene glycol terephthalate (PET) was kindly provided by Shanghai General Hospital. The polylactic acid (PLA, Mw = 110000, R055051–500g, RHAWN) was purchased from Shanghai Finder Technology Co., Ltd. The carbon fibers (CF) were kindly provided by the College of Materials Science and Engineering of Donghua University. Hexafluoroisopropanol (HFIP) was purchased from Shanghai Jiu Ming Trading Firm.

Table 1. qPCR Primer Sequence

| gene           | upstream primer        | downstream primer      |
|----------------|------------------------|------------------------|
| $\beta$ -actin | TGCTATGTTGCCCTAGACTTCG | GTTGGCATAGAGGTCTTTACGG |
| COL I          | AGAGGCATAAAGGGTCATCGTG | AGACCGTTGAGTCCATCTTTGC |
| TNC            | CAGAGTTGCCACCTACTTGCC  | TCTCTCCCTCATCTTTGTTC   |
| TNMD           | GTGTTTGGTATCTGGCCTTAA  | TGTTTCATCGGTGCCATTTT   |

The extraction method of silk fibroin (SF):  $\text{Na}_2\text{CO}_3$  of 30 g was dissolved in deionized water and boiled. Silkworm cocoons of 60 g were added and boiled for 30 min. The above steps were repeated three times to remove the sericin. The cocoons were torn and removed impurities. Then the boiled cocoons were dried. The LiBr of 273 g was dissolved in deionized water to 350 mL. The dried cocoons were added to the LiBr solution and stirred until completely dissolved. The solution was dialyzed in a  $1.4 \times 10^4$  dialysis bag for 3 days. Finally, the dialyzed solution was filtered and freeze-dried to obtain SF.

**2.2. Preparation of Scaffolds.** The CF was wrapped by nanofibers of PLA/SF to form a CF-mediated scaffold by conjugate electrospinning, this scaffold was named CPS (Figure 1). The preparation method was as follows: The PLA (1 g) and SF (1 g) were dissolved in 10 mL of HFIP. The solution was stirred at room temperature until complete dissolution. Two syringes containing solution were placed at the ends of the spinning machine and connected to the voltage. CF passed through the winding roller and was fixed on the receiving roller. After starting the machine, the nanofibers of PLA/SF from the spinning needle adhered to the CF under voltage to obtain the core-spun yarn. The three bundles of core-spun yarn were combined and spun again to obtain a thicker CF-mediated scaffold (CPS), in which the shell layer was PLA/SF nanofiber membrane (the number of core-spun yarns to be combined could be selected on demand). The first spinning parameters were: the voltage was 6.5 kV; the propulsion speed was 0.02 mL/min; the receiving roller speed was 8 rpm; and the winding roller speed was 400 rpm; the spinning needle was 20 G and the distance from the spinning needle to the winding roller was 10 cm. The spun again parameters were: the voltage was 6.5 kV; the propulsion speed was 0.05 mL/min; the receiving roller was 5 rpm; and the winding roller speed was 400 rpm; the spinning needle was 20 G and the distance from the spinning needle to the winding roller was 10 cm. Finally, CPS was cross-linked in 75% alcohol vapor for 3 days and then became more stable.

**2.3. Characterization of Scaffolds.** Scanning electron microscopy (SEM): the PET, CF, and CPS were prepared into a 10 mm sample and treated with a 6 mA ion sputtering current for 90 s. The samples were photographed at 140 X, 1000 X, and 3000 X to observe the surface and cross-section morphology. The SEM images were analyzed by Image-J software. The fibers of the scaffolds were randomly selected for diameter measurement ( $n = 3$ ).

Fourier transform infrared spectroscopy (FTIR): the functional groups of PLA and SF were analyzed by FTIR to verify whether the nanofibers of PLA/SF adhered to CF successfully ( $n = 3$ ).

Kelvin four-terminal sensing: the PET, CF, and CPS were prepared into a 40 mm sample. The thickness of the sample was measured, and then the resistivity was recorded. The conductivity  $\sigma$  (in S/m) was calculated using eq 1 ( $n = 3$ ):

$$\sigma = \frac{1}{\rho} \times 100 \quad (1)$$

where  $\rho$  is the resistivity (in  $\Omega\text{-cm}$ ).

Water contact angle test: PET, CF, and CPS were tightly fixed on slides. Water was dripped on the sample surface and the whole process was videotaped to record the water contact angle ( $n = 3$ ).

Mechanical test: PET, CF, and CPS were cut into 20 mm lengths, and the diameter of the sample was measured using a vernier card. The samples were fixed on the fixture of the tensile testing machine and the final length was measured. Uniaxial stretching was performed

at a tensile rate of 5 mm/min until the stress–strain curve dropped. The excel was obtained and the data was analyzed ( $n = 4$ ).

Thermogravimetric analysis (TGA): PET, CF, and CPS were weighed about 10 mg. The test parameters were: heating range was 50–800  $^\circ\text{C}$ , and heating rate was 10  $^\circ\text{C}/\text{min}$ . The thermal stability of the sample was analyzed after obtaining TGA curves ( $n = 3$ ).

*In vitro* degradation: CPS was weighed and exposed to UV light for 24 h. The sample was placed in Eppendorf tubes filled with sterile phosphate buffer solution and then placed in a shaker at 37  $^\circ\text{C}$ . After 1, 2, 4, 8, and 12 weeks, the samples were rinsed with deionized water. After freeze-drying, samples were measured for weight, SEM, and mechanical properties ( $n = 3$ ).

**2.4. Effects of ES on Cells *In Vitro*.** Tenocytes were extracted from two-week-old SD rats according to the previous report.<sup>29</sup> The SD rats were purchased from Shanghai JieSijie Laboratory Animal Co., Ltd. NIH 3T3 was obtained from the Cell Bank of the Chinese Academy of Sciences. Tenocytes were cultured in an incubator at 37  $^\circ\text{C}$ , 5%  $\text{CO}_2$ , and the medium (10% fetal bovine serum, 1% antibiotics, 89% MEM Alpha medium) was changed every 2 days. NIH 3T3 was cultured in an incubator at 37  $^\circ\text{C}$ , 5%  $\text{CO}_2$ , and the medium (10% fetal bovine serum, 1% antibiotics, 89% DMEM medium) was changed every 2 days.

Cell migration:  $5 \times 10^4$  tenocytes were seeded in six-well plates. After the tenocytes were spread all over the well plate, a scratch was made on the bottom with a 200  $\mu\text{L}$  tip. The tenocytes state without ES was photographed under an inverted fluorescence microscope. Then the tenocytes were given different intensities of ES for 1 h (0 mV, 0 mA; 10 mV, 1 mA; 10 mV, 5 mA; 10 mV, 10 mA), and the images were taken after the tenocytes were stabilized for about 3 h. After 12 h, the second ES was applied for 1 h, and the images were taken after 3 h. Serum-free medium with CCK-8 was prepared as a working solution in a ratio of 9:1. Then the working solution was added to the well plates and incubated for 1 h (37  $^\circ\text{C}$ , 5%  $\text{CO}_2$ ). Finally, the viability of the tenocytes was measured at the absorbance value of 450 nm.

Comparison of cells (tenocytes, NIH 3T3) without and with ES: PET, CF, and CPS were UV sterilized and transferred to 48-well plates. The  $2 \times 10^4$  cells were seeded in the three scaffolds and given 1 h of ES (10 mV, 1 mA) every day, while cells without ES served as control. Cell viability was tested and cell distribution was observed. After 7 days, the cells were fixed with 4% paraformaldehyde. After alcohol dehydration and drying, the cell adhesion on the scaffold was observed by SEM.

Expression of type I collagen (COL I) and tenomodulin (TNMD) of tenocytes *in vitro*: PET, CF, and CPS were UV sterilized and transferred to 12-well plates. The  $3 \times 10^4$  tenocytes were seeded in the three scaffolds and treated with 1 h of ES (10 mV, 1 mA) every day. The tenocytes were cultured for 10 days. Then the working solutions for immunofluorescence staining were prepared according to the instructions and the tenocytes were stained. Finally, photographs were taken under an inverted fluorescence microscope.

Quantitative real-time PCR (qPCR): PET, CF, and CPS were UV sterilized and transferred to 6-well plates. The  $1 \times 10^5$  tenocytes were seeded in the three scaffolds and given 1 h of ES (10 mV, 1 mA) every day. Then the tenocytes were cultured for 7 and 10 days and lysed from the scaffolds. Finally, according to the kit instructions and Table 1, the total RNA extraction, reverse transcription, and PCR amplification were performed. The data were analyzed according to the eqs 2–5.

$$\Delta\text{Ct}_{\text{exptl}} = \text{Ct}_{\text{target}} - \text{Ct}_{\text{ref}} \quad (2)$$

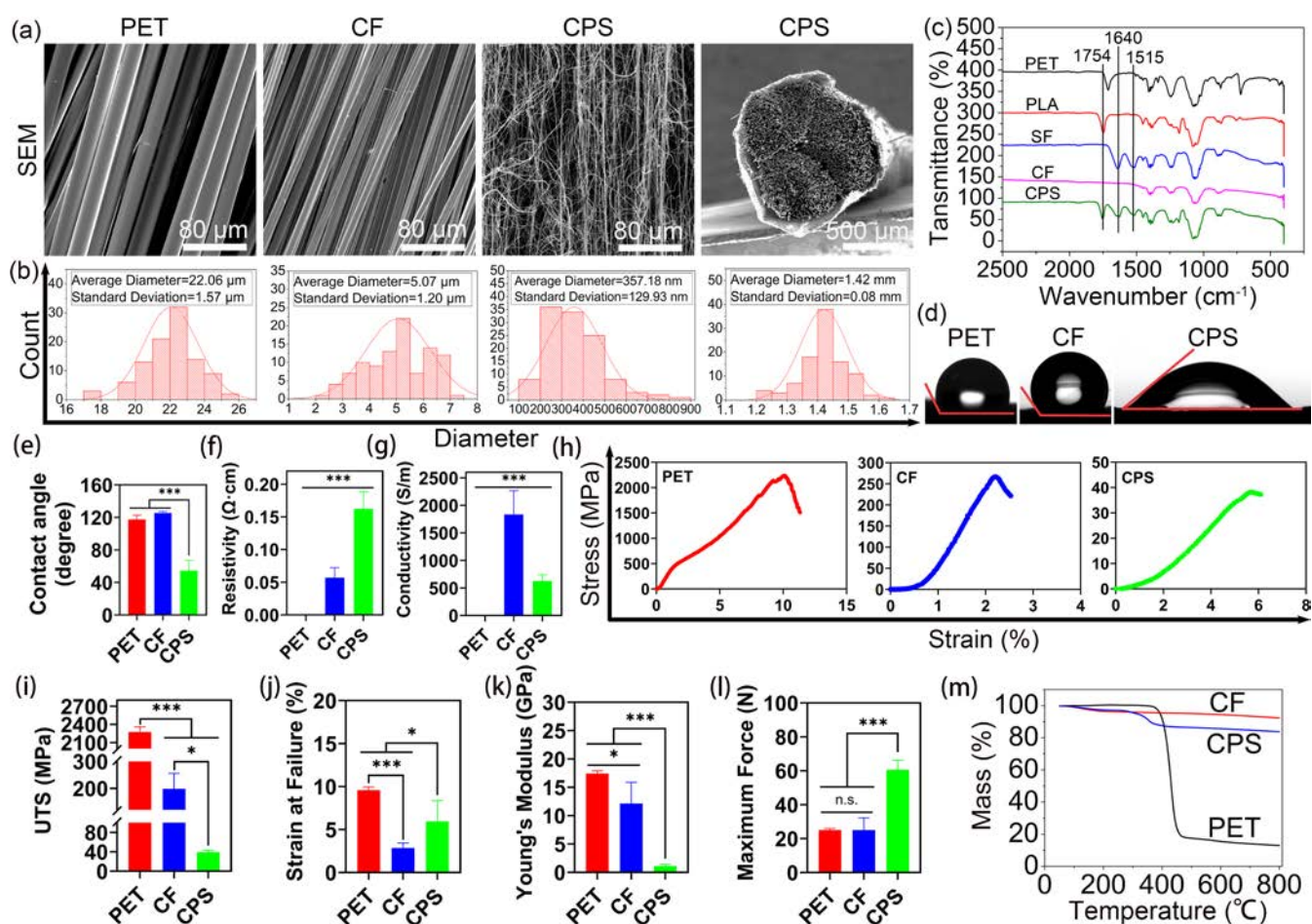


**Figure 2.** SEM images of PET, CF, and CPS (a) and corresponding diameter statistics (b), scale bar = 80  $\mu\text{m}$  and scale bar = 500  $\mu\text{m}$ . FTIR of PET, PLA, SF, CF, and CPS (c). Water contact angle measurement (d) and angle statistics (e) for PET, CF, and CPS. Resistivity (f) and conductivity (g) of PET, CF, and CPS. Mechanical testing of PET, CF, and CPS: stress–strain curve (h), ultimate tensile strength (UTS) (i), strain at failure (j), Young's modulus (k), and maximum force (l). TGA curves of PET, CF, and CPS (m). n.s.: no significance, \*  $p < 0.05$ , \*\*\*  $p < 0.001$ .

$$\Delta\text{Ct}_{\text{control}} = \text{Ct}_{\text{target}} - \text{Ct}_{\text{ref}} \quad (3)$$

$$\Delta\Delta\text{Ct} = \Delta\text{Ct}_{\text{exptl}} - \Delta\text{Ct}_{\text{control}} \quad (4)$$

$$\text{GER}_{\text{exptl}} = 2^{-\Delta\Delta\text{Ct}} \quad (5)$$

where  $\Delta\text{Ct}_{\text{exptl}}$  and  $\Delta\text{Ct}_{\text{control}}$  are  $\Delta\text{Ct}$  experimental group and  $\Delta\text{Ct}$  control group, respectively,  $\text{Ct}_{\text{target}}$  and  $\text{Ct}_{\text{ref}}$  are the Ct values for the target gene and internal reference gene, respectively, and  $\text{GER}_{\text{exptl}}$  is the gene expression rate for the experimental group.

**2.5. CPS Repaired Defective Tendons In Vivo.** This study passed the ethical approval of Chedun Experimental Animal Breeding Farm Co., Ltd., Songjiang, Shanghai (2023092010).

CPS was used *in vivo* to repair defective Achilles tendons in adult rabbits, while non-conductive PET nanoyarns made by conjugate electrospinning were used as a control, in which the shell layer was nanofiber membranes of PLA/SF and the core layer was PET. Each rabbit was injected with a dose of 0.3 mL/kg of Zoletil 50 via ear vein. After general anesthesia, the rabbit's left hind limb of the rabbit was shaved, sterilized, and the skin was incised to expose the Achilles tendon. A 1.5 mm  $\times$  15 mm defect was created in the Achilles tendon. The scaffold was embedded in the tendon defect and sutured to the surrounding tendon using a 6–0 suture. The Achilles tendon and skin were disinfected with iodophor. The skin was closed with 0 suture. Benzylpenicillin sodium was injected at  $4 \times 10^4$  units/kg approximately 3 times per day for 3 days.

After the surgery, each rabbit was individually housed in a cage with sufficient space to allow for free movement, and the rabbits'

movements were observed and recorded regularly. The prognosis functional scoring of the rabbit Achilles tendon was assessed according to the Thompson test, the Leppilahti scoring system, and the actual situation.<sup>30</sup> The repaired Achilles tendon samples at 4 and 12 weeks were treated with hematoxylin-eosin (HE) staining, Masson's trichrome (MT) staining, and transcriptome sequencing (RNA-seq). The histological score of HE staining was calculated according to the semi-quantitative histology scoring system.<sup>31</sup> The collagen spreading area of MT staining was calculated using Image-J software.

**2.6. Statistical Analysis.** All data were expressed as mean  $\pm$  standard deviation from three independent experiments with a minimum of three replicates for each condition. One-way analysis of variance (ANOVA) followed by Tukey's post hoc test was used to determine the statistical significance unless specified otherwise. The significant difference was considered at \*  $p < 0.05$  and \*\*  $p < 0.01$ , \*\*\*  $p < 0.001$ .

### 3. RESULTS

**3.1. Characteristics of Scaffolds.** It was observed under the SEM that PET and CF were composed of many bundled monofilaments. PET monofilament diameter was  $22.06 \pm 1.57$   $\mu\text{m}$  and CF monofilament diameter was  $5.07 \pm 1.20$   $\mu\text{m}$ . CPS was composed of three core-spun yarns with a thick nanofiber membrane on the outside, so the CPS was not easy to lose. The diameter of CPS was  $1.42 \pm 0.08$  mm and the diameter of nanofibers on its surface was  $357.18 \pm 129.93$  nm (Figure

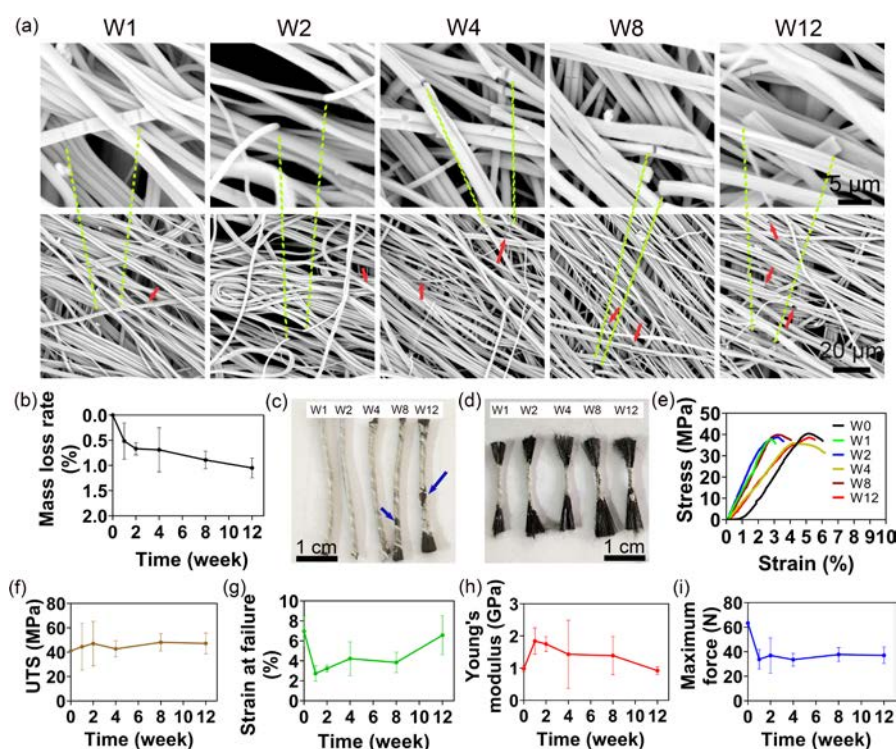


**Figure 3.** Degradation of CPS after 1, 2, 4, 8, and 12 weeks. SEM (a), scale bar = 5  $\mu\text{m}$ , and scale bar = 20  $\mu\text{m}$ . Mass loss rate (b). Macroscopic view after freeze-drying (c), and the macroscopic view after mechanical stretching (d), scale bar = 1 cm. The stress–strain curve (e), UTS (f), strain at failure (g), Young's modulus (h), and maximum force (i). Yellow-green dotted line: enlarged view of nanofiber fracture. Red arrow: other nanofiber fracture. Blue arrow: shed nanofiber membrane.

2a,b). From the FTIR, it could be seen that the nanofiber membranes of PLA/SF were successfully spun on CF to form CPS (Figure 2c).

As shown by the water contact angle, PET and CF were hydrophobic, while the surface of CPS was hydrophilic due to the SF-containing nanofiber membrane on the surface (Figure 2d,e). The resistivity of PET was very high, so it was not conductive (beyond the measurement range of the instrument, so the picture was blank). The resistivity of CF was  $0.0569 \pm 0.0154 \Omega\cdot\text{cm}$ , and the conductivity was  $1833.80 \pm 429.22 \text{ S/m}$ . The resistivity of CPS was  $0.1623 \pm 0.0264 \Omega\cdot\text{cm}$ , and the conductivity was  $627.87 \pm 109.71 \text{ S/m}$ . Due to the nanofiber membrane on the surface of CPS, the resistivity of CPS increased and the conductivity decreased compared with CF (Figure 2f,g).

When the stress–strain curve dropped, all scaffolds did not exhibit intermediate fractures, but rather fractures or bulges in the monofilament parts of PET and CF, while the scaffolds of CPS showed bulges or cracks in the nanofibers on their surface. At this time, the UTS on PET was  $2273 \pm 89.34 \text{ MPa}$  and the strain was  $9.59 \pm 0.34\%$ , Young's modulus of PET was  $17.45 \pm 0.46 \text{ GPa}$ , and the maximum force was  $25.01 \pm 0.98 \text{ N}$ . The UTS on CF was  $198.69 \pm 56.84 \text{ MPa}$  and the strain was  $2.85 \pm 0.58\%$ , Young's modulus of CF was  $12.15 \pm 3.74 \text{ GPa}$ , and the maximum force was  $25.04 \pm 7.16 \text{ N}$ . The UTS on CPS was  $39.38 \pm 3.65 \text{ MPa}$  and the strain was  $5.95 \pm 2.41\%$ , Young's modulus of CPS was  $1.12 \pm 0.29 \text{ GPa}$ , and the maximum force was  $60.61 \pm 5.62 \text{ N}$  (Figure 2h–l and Table S1–S3). The mechanics of the three scaffolds were quite different, among which CPS was the weakest in some aspects, but it was the largest in maximum force. This phenomenon occurred mainly because the surface nanofiber membrane of

CPS bulged under the action of external force. However, the role of the nanofiber membrane was mainly to wrap the CF into a whole that was not easily dispersed, and the main load-bearing was the reinforced core CF. Therefore, Compared to the human Achilles tendon,<sup>32</sup> the mechanical properties of CPS were sufficient for practical applications.

The TGA curves showed that the mass loss of PET at 450  $^{\circ}\text{C}$  was  $76.06 \pm 0.18\%$ . The mass loss of CF at 400  $^{\circ}\text{C}$  was  $4.56 \pm 0.001\%$ , while that of CPS was  $12.49 \pm 0.01\%$ , and more mass loss came from the nanofiber membrane on the surface of CPS. It could be seen that three scaffolds had good thermal stability (Figure 2m).

PET and CF were nondegradable, while the nanofiber membrane on the surface of CPS was degradable. Therefore, it was necessary to research the CPS properties of nanofiber membrane after degradation. After the first week, cracks appeared in the nanofibers, and the number of fractured fibers gradually increased from 2 weeks to 12 weeks (Figure 3a). After 12 weeks, the mass loss of CPS was  $1.05 \pm 0.19\%$  (Figure 3b). At 1 to 4 weeks, the mass loss of CPS was mainly from the degradation of materials in the nanofiber membrane. At 8 weeks, the nanofiber membrane showed signs of shedding. At 12 weeks, the shed nanofiber membrane was visible, and the mass loss also included the shed nanofiber membrane (Figure 3c). The CPS were stretched until the stress–strain curve dropped, at which point the nanofiber membrane was visible shedding from the CF, rather than the fracture of CPS. Therefore, at this point, it was the force of the nanofiber membrane shedding from the CPS (Figure 3d). Compared to the human Achilles tendon,<sup>32</sup> the mechanical properties of CPS at all time points fluctuated within a stable range and showed good mechanical properties to meet the subsequent

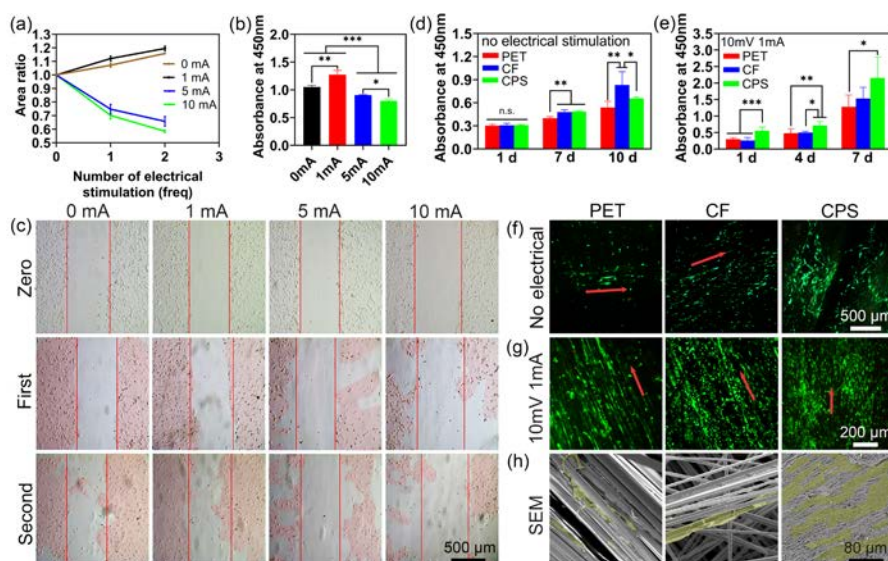


**Figure 4.** Migration of tenocytes under different levels of ES: spreading area ratio change after ES (a), the CCK – 8 after the second ES (b), the spreading of tenocytes after the 0th, first, and second ES (c), scale bar = 500  $\mu\text{m}$ . Tenocytes proliferation after 1, 7, and 10 days without ES (d). Tenocytes live/dead staining after 7 days of 10 mV, 1 mA ES (e). Tenocytes live/dead staining after 7 days of 10 mV, 1 mA ES (g), scale bar = 200  $\mu\text{m}$ . SEM of tenocytes adhesion on the surface of the PET, CF, and CPS scaffold (h), scale bar = 80  $\mu\text{m}$ . Red arrow: direction of tenocytes alignment. n.s.: no significance, \*  $p < 0.05$ , \*\*  $p < 0.01$ , \*\*\*  $p < 0.001$ .

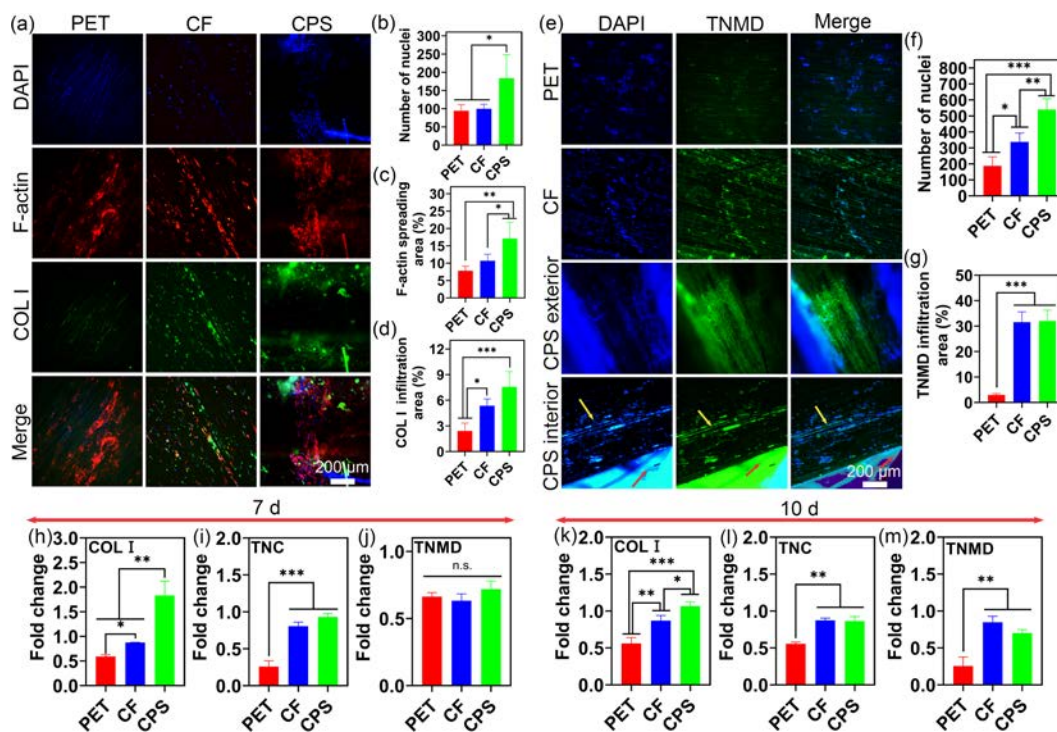


**Figure 5.** DAPI/F-actin/COL I immunofluorescence staining of tenocytes cultured on PET, CF, CPS scaffolds for 10 days with 10 mV, 1 mA ES (a), scale bar = 200  $\mu\text{m}$ , and the statistics of number of nuclei (b), F-actin spreading area (c), COL I infiltration area (d). DAPI/TNMD immunofluorescence staining of tenocytes cultured on PET, CF, CPS scaffolds for 10 days with 10 mV, 1 mA ES (e), scale bar = 200  $\mu\text{m}$ , and the statistics of number of nuclei (f), TNMD infiltration area (g). The gene expression of the tenocytes cultured on the PET, CF, and CPS scaffolds with 10 mV, 1 mA ES after 7 days was tested by qPCR: COL I (h), TNC (i), and TNMD (j). The gene expression of the tenocytes cultured on the PET, CF, and CPS scaffolds with 10 mV, 1 mA ES after 10 days was tested by qPCR: COL I (k), TNC (l), and TNMD (m). Yellow arrow: the CF inside the CPS. Red arrow: the nanofiber membrane on the CPS surface. n.s.: no significance, \*  $p < 0.05$ , \*\*  $p < 0.01$ , \*\*\*  $p < 0.001$ .

experimental requirements (Figure 3e–i). Since there were signs of nanofiber membrane shedding and CF was gradually exposed from the 8 weeks, the conductivity of CPS also began to increase, especially in the 12 weeks (Figure S4).

**3.2. In Vitro ES Affected Cell Migration, Proliferation, and Alignment.** Different intensities of ES could affect tenocytes migration ability. The migration test showed that the tenocytes spreading area and viability increased when the current was 1 mA. However, the tenocytes spreading area and

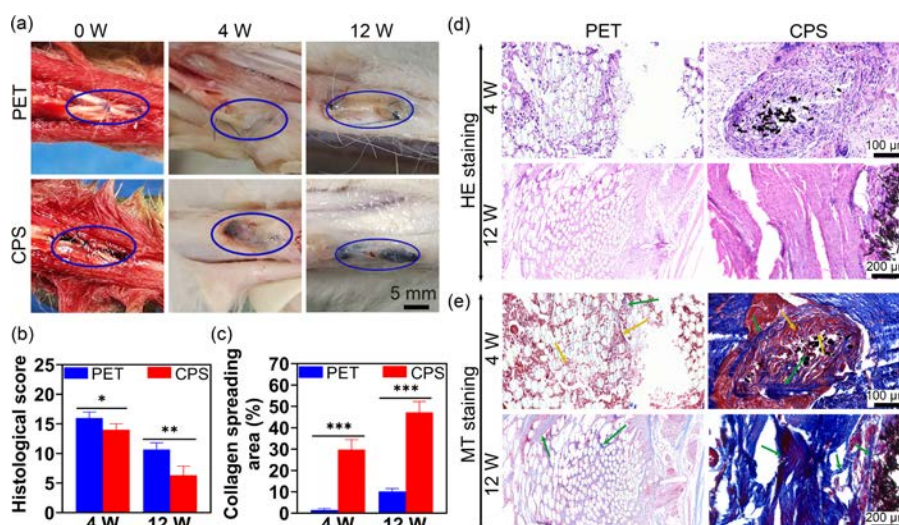


**Figure 6.** Repair of defective Achilles tendon. Macroscopic view of PET and CPS scaffold implantation in the defect area after 0, 4, and 12 weeks (a), scale bar = 5 mm, histological score (b), collagen spreading area (c), HE staining (d) and MT staining (e), scale bar = 100  $\mu\text{m}$ , and scale bar = 200  $\mu\text{m}$ . Orange arrow: muscle fibers. Green arrow: collagen fibers. \*  $p < 0.05$ , \*\*  $p < 0.01$ , \*\*\*  $p < 0.001$ .

viability were decreased due to the excessive current of 5 mA and 10 mA after the second ES. The above indicated that the micro-ES was conducive to tenocytes migration (Figure 4a–c).

ES could affect tenocytes proliferation ability. The tenocytes viability with ES after 7 days had exceeded that of the without ES after 10 days (Figure 4d,e). There were three phenomena worth noting among them: first, the tenocytes survived better on CF after 10 days without ES. Second, the tenocytes were better able to adapt to the CPS and proliferate rapidly at any time point in the presence of ES. Third, due to the conductivity of the culture medium, tenocytes proliferated faster with ES than without ES on non-conductive PET. These indicated that, on the one hand, the nanofiber membrane on the surface of CPS reduced conductivity, providing time for tenocytes to adapt to the current, thereby protecting tenocytes and promoting growth more quickly. On the other hand, appropriate micro-ES could indeed promote tenocytes proliferation.

ES could affect tenocytes alignment ability. In the absence of ES, the tenocytes were randomly arranged on the CPS, while in the presence of ES, the tenocytes could be arranged regularly along the direction of the current (Figure 4f,g). Through SEM, it could be seen that tenocytes could cover the surface of CPS (Figure 4h).

In order to rule out the possibility that ES only affected tenocytes, the experiment found that NIH 3T3 also obtained similar results under ES: the nanofiber membrane on the surface of CPS had a protective effect on NIH 3T3, and the ES could cause the NIH 3T3 to align directionally on the CPS surface (Figure S5).

**3.3. CPS Could Better Promote the Expression of Tenocytes.** The immunofluorescence staining of DAPI/F-actin/COL I showed that tenocytes proliferated fastest on CPS (Figure 5a–c). Among them, the tenocytes spread out along the direction of PET and CF, and more collagen was expressed on the CF scaffold than on PET (Figure 5a,d). In the CPS, two CPS were covered with tenocytes and a large amount of collagen appeared (Figure 5a,d). Interestingly, a small number of tenocytes appeared in the gap between the two CPS, indicating that the tenocytes between the CPS could attract each other and had just established a connection. Although

there was no collagen expression here yet, it was only a matter of time (Figure 5a). Similar results were also obtained by immunofluorescence staining for DAPI/TNMD: tenocytes proliferated faster on CPS (Figure 5e,f). The expression of TNMD in CF and CPS was much higher than that in PET (Figure 5g). It was worth noting that tenocytes appeared inside CPS and TNMD expression was observed when the CPS was cut open (Figure 5e).

According to qPCR, the most collagen was expressed on the CPS at both 7 and 10 days (Figure 5h,k). There was no significant difference in TNC expression between CF and CPS, but both were higher than PET (Figure 5i,l). TNMD expression on the scaffolds was not significantly different at 7 days, but after 10 days, the scaffolds of CF and CPS had more TNMD expression than PET (Figure 5j,m). From the above tests, it could be seen that in the case of appropriate ES, CPS could not only promote the rapid proliferation of tenocytes but also better enhance the COL I, TNC, and TNMD expression.

**3.4. CPS Repaired Defective Tendons *In Vivo*.** PET nanofibers and CPS were implanted into the Achilles tendon defects in rabbits, and after 4 and 12 weeks, the rabbits with CPS scaffolds had better mobility recovery than those with PET (Figure S6). After dissection, it was found that the surface of the scaffolds was covered with a thin layer of tissue after 4 and 12 weeks (Figure 6a). From the HE staining, it could be seen that the cells had grown into the interior of PET and CPS scaffolds after 4 weeks. The CPS was repaired faster than the PET scaffold for tendons at 4 and 12 weeks (Figure 6b,d). From the MT staining at 4 weeks, the expression of muscle fibers and collagen fibers was accompanied by CPS, but there was almost no expression of collagen fibers around PET scaffolds. Similarly, it could be seen that CPS was surrounded by collagen fibers after 12 weeks, while only a small amount of collagen fibers appeared around PET, indicating that CPS was more conducive to the growth of tendon tissue (Figure 6c,e).

**3.5. Conductive CPS Accelerated Fibromodulin (FMOD) and TNMD Expression *In Vivo*.** To evaluate the potential mechanism of conductive CPS in the repair of defective tendons under the action of endogenous electric field in the organism, the new tissue after PET nanofibers and CPS repair was analyzed by RNA-seq. There were significant genetic

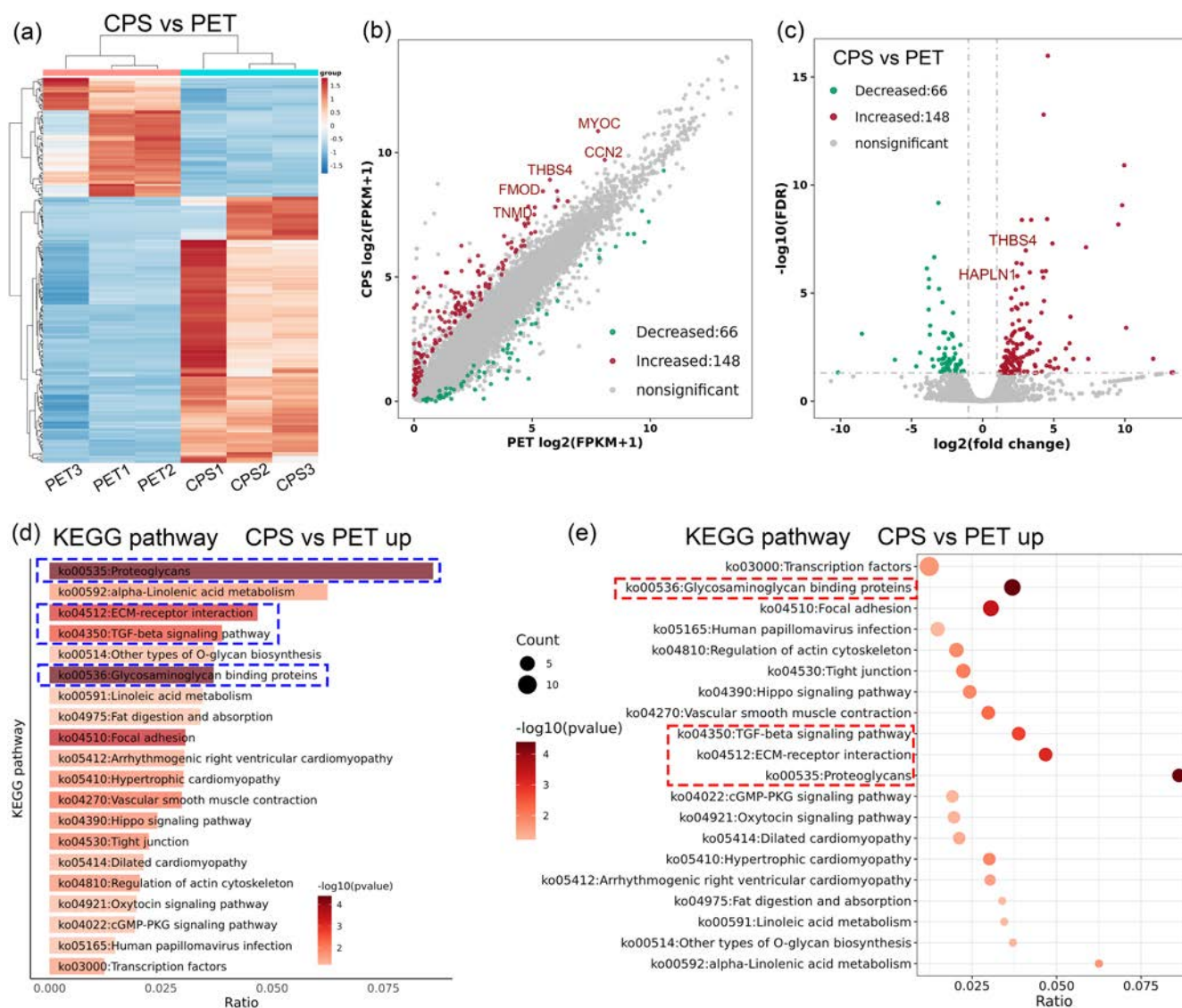


**Figure 7.** RNA-seq of CPS and PET repaired tendon. Differential gene clustering heat map (a), differential gene expression scatter plot (b), differential gene expression volcano map (c), KEGG pathway enrichment analysis bar graph (d), KEGG enrichment analysis bubble chart (e).

differences between the newly formed tissues of CPS and PET as seen by the heat map (Figure 7a). Specifically, FMOD and TNMD that affected tendon repair were upregulated in CPS compared to PET (Figure 7b). In addition, myocilin (MYOC), connective tissue growth factor (CCN2), thrombospondin 4 (THBS4), hyaluronan and proteoglycan link protein 1 (HAPLN1) related to tissue repair were also upregulated (Figure 7b,c). Further analysis revealed that the FMOD and TNMD-associated proteoglycans and glycosaminoglycan binding proteins pathways were enhanced, which were closely related to the TGF- $\beta$  signaling pathway, and optimized the assembly of the extracellular matrix (ECM) to promote tendon repair (Figure 7d,e).

#### 4. DISCUSSION

Tendons have piezoelectric properties, and bioelectric signals play an important role in promoting tendon-specific phenotypes, which can be manifested in gene and protein expression, biological function, pathway analysis, and other aspects.<sup>10,33</sup> Zhang et al.<sup>34</sup> researched a piezoelectric nanofiber scaffold that combined exercise-driven ES and nanotopological

effects to promote tendon-to-bone healing. Conductive materials have been widely used in nerve, myocardial, bone, and skin repair, but few have been used in tendon defect repair.<sup>35–37</sup> Therefore, the potential of activating tendon-specific phenotypes to promote tendon repair by conducting bioelectric signals *in vivo* through microcurrents generated by conductive materials needs to be explored. CF is an ideal reinforcement material because of its high strength and high modulus. In addition, CF has excellent electrical conductivity, which is even close to the metal.<sup>38</sup> At the same time, CF can also form conductive microcircuits to stimulate tissue growth.<sup>39</sup> Chua et al.<sup>40</sup> designed CF-reinforced polymers for implantable medical devices and found that they had good biocompatibility *in vivo*. Green et al.<sup>41</sup> found that collagen/CF had a structure similar to that of natural tendons. Interestingly, in this study, the diameter of the CF monofilament was close to that of the collagen fibers in the tendon, which helped to conduct electrical signals (Figure 2a,b). Meanwhile, cell tests also demonstrated that appropriate ES could promote the migration, proliferation, and orientation alignment of tenocytes

(Figure 4a–g). Therefore, CF is potentially useful in tendon repair.

In this study, CF-mediated scaffolds were prepared by electrospinning (Figure 1). Nanofiber membrane wrapped CF so that it was not easily loosened and could become a complete scaffold (Figure 2a). It was found that the maximum force of the CPS was much greater than that of CF scaffold. This was because during the stretching process, when the stress–strain curve decreased, the monofilaments in the CF scaffold appeared to break, and the CPS was the nanofiber membrane bulging or falling off, so the presence of nanofiber membrane could protect the monofilaments of the CF reinforcing core (Figure 2l). At the same time, the nanofiber membrane increased the hydrophilicity of the CPS, which provided a good condition for cell adhesion and proliferation (Figure 2d,e). Cell experiments showed that under appropriate ES, the nanofiber membrane on the surface of CPS reduced conductivity, providing time for tenocytes to adapt to the microcurrent, and thus protecting tenocytes, so that the tenocytes proliferated faster than PET and CF scaffolds at any time point (Figures 2f,g and 4e). In addition, the presence of nanofiber membranes expanded the surface area of the CPS, and more tenocytes were attached to the surface and interior of the scaffold, providing a larger space for rapid tenocytes proliferation and TNMD expression than PET (Figure 5e–g).

Although carbon-based materials are nondegradable, the benefits of using conductive carbon-based components may outweigh the disadvantages found in most studies for tissue regeneration.<sup>42</sup> In this study, the nanofiber membrane on the surface of CPS was degradable. As the nanofiber degraded, tissue gradually replaced the nanofiber membrane and changed from nanofiber membrane-wrapped CF to tissue-wrapped CF, which was beneficial for CF to play a long-term conductive role *in vivo*. The mechanics of the CPS fluctuated steadily within a certain range in the degradation tests, and the scaffolds did not detach from the tissue in the animal tests, which showed that the mechanical properties of the scaffold were matched to the Achilles tendon of the rabbits (Figures 3e–i and 6a).

Tenocytes were seeded on PET, CF, and CPS scaffolds and given ES. CPS could accelerate the expression of tenocytes-related proteins and genes, such as COL I, TNC, and TNMD (Figure 5). This was confirmed in animal experiments, the CPS around the defect tendon was covered with new tissue and collagen fibers at a higher rate than the non-conductive PET nanoyarns due to the presence of the endogenous electric field in the animal (Figure 6b,c). TNMD is a type II transmembrane glycoprotein containing a highly conserved c-terminal cysteine-rich structural domain that co-localizes with type I collagen fibrils into the ECM of tendons after cleavage.<sup>43</sup> TNMD is the most well-known marker of maturation of tendon lineage cells, which has great significance for tendon maturation, motility, and resident tendon stem/progenitor cells.<sup>44</sup> FMOD in proteoglycans is required for the formation of normal collagen fibers and the cross-linking of collagen. In acute tendon injury models, an increase in FMOD can promote tendon healing.<sup>45</sup> Consequently, the expression of FMOD and TNMD is essential for collagen repair in tendons. Through RNA-seq of the newly formed tissues, it could be seen that the expression of FMOD and TNMD was upregulated, indicating that the tissue growing around the CPS was more tendon tissue (Figure 7b). During tissue repair, the TGF- $\beta$  signaling pathway is activated, which can promote the production of collagen in tenocytes, and closely

communicate with tendon-related genes such as FMOD and TNMD.<sup>46–48</sup> FMOD subtly coordinates TGF- $\beta$  signal transduction. FMOD selectively enhances early pro-migration and pro-contraction TGF- $\beta$ 1 signaling to reduce scar size and increase wound tissue tensile strength, while inhibiting TGF- $\beta$ -stimulated fibrosis gene expression to reduce scar tissue formation.<sup>48</sup> During RNA-seq, the expression of FMOD and TNMD-associated proteoglycans and glycosaminoglycan binding proteins was enhanced, the closely related TGF- $\beta$  signaling pathway was activated, and both the ECM receptor interaction was upregulated, indicating that under the action of endogenous electric fields, CPS could promote repair by activating various pathways through conducting electrical signaling (Figure 7d,e).

There are some shortcomings in this study. Due to the high hardness and strength of the CF as a reinforcing core, when sections of animal tissues were obtained, the machine's knife did not cut well and the number of sections obtained was limited, resulting in many validation tests not being completed. In the next step, we will focus on the development of degradable conductive scaffolds with good mechanical properties for the repair of defective tendons and deepen more validation experiments.

## 5. CONCLUSIONS

In this study, the carbon fiber-mediated electrospinning scaffolds were designed. The diameter of the reinforcing core CF in this CPS was similar to that of collagen fibers, which could facilitate the rapid recovery of the disappeared endogenous electric field of the defective tendon *in vivo*. The nanofiber membrane on the surface of CPS could help tenocytes adapt to ES, and accelerate proliferation and expression. The rabbit Achilles tendon defect test showed that the CPS was more conducive to collagen fiber production. Through RNA-seq, it was found that tendon repair was associated with the TGF- $\beta$  signaling pathway, and CPS upregulated the expression of FMOD and TNMD, which together promoted tendon repair.

## ■ ASSOCIATED CONTENT

### Supporting Information

The Supporting Information is available free of charge at <https://pubs.acs.org/doi/10.1021/acsami.4c12245>.

Table S1: PET mechanical test data. Table S2: CF mechanical test data. Table S3: CPS mechanical test data. Figure S4: Change in conductivity after degradation. Figure S5: Comparison of NIH 3T3 without and with ES. Figure S6: The prognosis of the rabbit Achilles tendon (PDF)

## ■ AUTHOR INFORMATION

### Corresponding Authors

Xiumei Mo – State Key Laboratory for Modification of Chemical Fibers and Polymer Materials, Shanghai Engineering Research Center of Nano-Biomaterials and Regenerative Medicine, College of Biological Science and Medical Engineering, Donghua University, Shanghai 201620, China; [orcid.org/0000-0001-9238-6171](https://orcid.org/0000-0001-9238-6171); Email: [xmm@dhu.edu.cn](mailto:xmm@dhu.edu.cn)

Binbin Sun – State Key Laboratory for Modification of Chemical Fibers and Polymer Materials, Shanghai Engineering Research Center of Nano-Biomaterials and

Regenerative Medicine, College of Biological Science and Medical Engineering, Donghua University, Shanghai 201620, China; Email: [binbin.sun@dhu.edu.cn](mailto:binbin.sun@dhu.edu.cn)

**Yinxian Yu** – Department of Orthopedic Surgery, Shanghai General Hospital, Shanghai Jiao Tong University School of Medicine, Shanghai 200240, China; Email: [eastpool@sjtu.edu.cn](mailto:eastpool@sjtu.edu.cn)

## Authors

**Xiao Yu** – State Key Laboratory for Modification of Chemical Fibers and Polymer Materials, Shanghai Engineering Research Center of Nano-Biomaterials and Regenerative Medicine, College of Biological Science and Medical Engineering, Donghua University, Shanghai 201620, China

**Genbin Wu** – Department of Orthopedic Surgery, Shanghai General Hospital, Shanghai Jiao Tong University School of Medicine, Shanghai 200240, China

**Pengfei Cai** – State Key Laboratory for Modification of Chemical Fibers and Polymer Materials, Shanghai Engineering Research Center of Nano-Biomaterials and Regenerative Medicine, College of Biological Science and Medical Engineering, Donghua University, Shanghai 201620, China

**Yangfan Ding** – State Key Laboratory for Modification of Chemical Fibers and Polymer Materials, Shanghai Engineering Research Center of Nano-Biomaterials and Regenerative Medicine, College of Biological Science and Medical Engineering, Donghua University, Shanghai 201620, China

**Jie Cui** – State Key Laboratory for Modification of Chemical Fibers and Polymer Materials, Shanghai Engineering Research Center of Nano-Biomaterials and Regenerative Medicine, College of Biological Science and Medical Engineering, Donghua University, Shanghai 201620, China

**Jinglei Wu** – State Key Laboratory for Modification of Chemical Fibers and Polymer Materials, Shanghai Engineering Research Center of Nano-Biomaterials and Regenerative Medicine, College of Biological Science and Medical Engineering, Donghua University, Shanghai 201620, China; [orcid.org/0000-0001-9549-3992](https://orcid.org/0000-0001-9549-3992)

**Yihong Shen** – State Key Laboratory for Modification of Chemical Fibers and Polymer Materials, Shanghai Engineering Research Center of Nano-Biomaterials and Regenerative Medicine, College of Biological Science and Medical Engineering, Donghua University, Shanghai 201620, China

**Jiahui Song** – State Key Laboratory for Modification of Chemical Fibers and Polymer Materials, Shanghai Engineering Research Center of Nano-Biomaterials and Regenerative Medicine, College of Biological Science and Medical Engineering, Donghua University, Shanghai 201620, China

**Zhengchao Yuan** – State Key Laboratory for Modification of Chemical Fibers and Polymer Materials, Shanghai Engineering Research Center of Nano-Biomaterials and Regenerative Medicine, College of Biological Science and Medical Engineering, Donghua University, Shanghai 201620, China

**Mohamed EL-Newehy** – Department of Chemistry, College of Science, King Saud University, Riyadh 11451, Saudi Arabia

**Meera Moydeen Abdulhameed** – Department of Chemistry, College of Science, King Saud University, Riyadh 11451, Saudi Arabia

**Huifang Chen** – College of Materials Science and Engineering and State Key Laboratory for Modification of Chemical Fibers and Polymer Materials, Donghua University, Shanghai 201620, China; [orcid.org/0000-0002-6314-455X](https://orcid.org/0000-0002-6314-455X)

Complete contact information is available at: <https://pubs.acs.org/10.1021/acsami.4c12245>

## Author Contributions

<sup>†</sup>X.Y. and G.W. contributed equally to this work.

## Notes

The authors declare no competing financial interest.

## ACKNOWLEDGMENTS

This project was supported by the Fundamental Research Funds for the Central Universities (CUSF-DH-T-2023063), Shanghai Committee of Science and Technology (23ZR1451700), Science and Technology Commission of Shanghai Municipality, China (20DZ2254900), Sino German Science Foundation Research Exchange Center, China (M-0263), and China Education Association for International Exchange (2022181). This project was also supported by Researchers Supporting Project Number (RSP2024R65), King Saud University, Riyadh, Saudi Arabia. This project was also supported by the grants from the National Natural Science Foundation of China (82302687), and Medicine-Engineering Interdisciplinary Project of Shanghai Jiao Tong University (YG2022QN076).

## REFERENCES

- (1) Zhang, Y.; Xue, Y.; Ren, Y.; Li, X.; Liu, Y. Biodegradable Polymer Electrospinning for Tendon Repairment. *Polymers* **2023**, *15* (6), 1566.
- (2) Cai, J.; Xu, J.; Ye, Z.; Wang, L.; Zheng, T.; Zhang, T.; Li, Y.; Jiang, J.; Zhao, J. Exosomes Derived From Kartogenin-Preconditioned Mesenchymal Stem Cells Promote Cartilage Formation and Collagen Maturation for Enthesis Regeneration in a Rat Model of Chronic Rotator Cuff Tear. *Am. J. Sports Med.* **2023**, *51* (5), 1267–1276.
- (3) Yu, X.; Cui, J.; Shen, Y.; Guo, W.; Cai, P.; Chen, Y.; Yuan, Z.; Liu, M.; El-Newehy, M.; El-Hamshary, H.; et al. Current Advancements and Strategies of Biomaterials for Tendon Repair: A Review. *Front Biosci.* **2023**, *28* (4), 66.
- (4) Wang, J. H. Mechanobiology of tendon. *J. Biomech.* **2006**, *39* (9), 1563–1582.
- (5) Gracey, E.; Burssens, A.; Cambre, I.; Schett, G.; Lories, R.; McInnes, I. B.; Asahara, H.; Elewaut, D. Tendon and ligament mechanical loading in the pathogenesis of inflammatory arthritis. *Nat. Rev. Rheumatol.* **2020**, *16* (4), 193–207.
- (6) Yang, Q.; Li, J.; Su, W.; Yu, L.; Li, T.; Wang, Y.; Zhang, K.; Wu, Y.; Wang, L. Electrospun aligned poly(epsilon-caprolactone) nanofiber yarns guiding 3D organization of tendon stem/progenitor cells in tenogenic differentiation and tendon repair. *Front. Bioeng. Biotechnol.* **2022**, *10*, 960694.
- (7) Kim, D.; Han, S. A.; Kim, J. H.; Lee, J.-H.; Kim, S.-W.; Lee, S.-W. Biomolecular Piezoelectric Materials: From Amino Acids to Living Tissues. *Adv. Mater.* **2020**, *32* (14), No. e1906989.
- (8) Bassett, C. A. L. Biologic significance of piezoelectricity. *Calcified Tissue Res.* **1967**, *1* (1), 252–272.
- (9) Wang, J.; Lin, J.; Chen, L.; Deng, L.; Cui, W. Endogenous Electric-Field-Coupled Electrospun Short Fiber via Collecting Wound Exudation. *Adv. Mater.* **2022**, *34* (9), No. e2108325.
- (10) Fernandez-Yague, M. A.; Trotier, A.; Demir, S.; Abbah, S. A.; Larranaga, A.; Thirumaran, A.; Stapleton, A.; Tofail, S. A. M.; Palma, M.; Kilcoyne, M.; Pandit, A.; Biggs, M. J. A Self-Powered Piezo-Bioelectric Device Regulates Tendon Repair-Associated Signaling

Pathways through Modulation of Mechanosensitive Ion Channels. *Adv. Mater.* **2021**, *33* (40), No. e2008788.

(11) Alvarez-Lorenzo, C.; Zarur, M.; Seijo-Rabina, A.; Blanco-Fernandez, B.; Rodríguez-Moldes, I.; Concheiro, A. Physical stimuli-emitting scaffolds: The role of piezoelectricity in tissue regeneration. *Mater. Today Bio.* **2023**, *22*, 100740.

(12) Leek, C. C.; Soulas, J. M.; Sullivan, A. L.; Killian, M. L. Using tools in mechanobiology to repair tendons. *Curr. Tissue Microenviron Rep.* **2020**, *1* (2), 31–40.

(13) Chen, C.; Bai, X.; Ding, Y.; Lee, I.-S. Electrical stimulation as a novel tool for regulating cell behavior in tissue engineering. *Biomater. Res.* **2019**, *23* (1), 25.

(14) Leppik, L.; Oliveira, K. M. C.; Bhavsar, M. B.; Barker, J. H. Electrical stimulation in bone tissue engineering treatments. *Eur. J. Trauma Emerg Surg.* **2020**, *46* (2), 231–244.

(15) Sun, B.; Wu, T.; Wang, J.; Li, D.; Wang, J.; Gao, Q.; Bhattu, M. A.; El-Hamshary, H.; Al-Deyab, S. S.; Mo, X. Polypyrrole-coated poly(l-lactic acid-co-epsilon-caprolactone)/silk fibroin nanofibrous membranes promoting neural cell proliferation and differentiation with electrical stimulation. *J. Mater. Chem. B.S.* **2016**, *4* (41), 6670–6679.

(16) Kwon, H. J.; Lee, G. S.; Chun, H. Electrical stimulation drives chondrogenesis of mesenchymal stem cells in the absence of exogenous growth factors. *Sci. Rep.* **2016**, *6*, 39302.

(17) de Campos Ciccone, C.; Zuzzi, D. C.; Neves, L. M. G.; Mendonça, J. S.; Joazeiro, P. P.; Esquisatto, M. A. M. Effects of microcurrent stimulation on Hyaline cartilage repair in immature male rats (*Rattus norvegicus*). *BMC Complementary Altern. Med.* **2013**, *13*, 17.

(18) Zhang, H.; Lan, D.; Wu, B.; Chen, X.; Li, X.; Li, Z.; Dai, F. Electrospun Piezoelectric Scaffold with External Mechanical Stimulation for Promoting Regeneration of Peripheral Nerve Injury. *Biomacromolecules* **2023**, *24* (7), 3268–3282.

(19) Ferrigno, B.; Bordett, R.; Duraisamy, N.; Moskow, J.; Arul, M. R.; Rudraiah, S.; Nukavarapu, S. P.; Vella, A. T.; Kumbar, S. G. Bioactive polymeric materials and electrical stimulation strategies for musculoskeletal tissue repair and regeneration. *Bioact. Mater.* **2020**, *5* (3), 468–485.

(20) No, Y. J.; Castilho, M.; Ramaswamy, Y.; Zreiqat, H. Role of Biomaterials and Controlled Architecture on Tendon/Ligament Repair and Regeneration. *Adv. Mater.* **2020**, *32* (18), No. e1904511.

(21) Jenkins, D.; McKibbin, B. The role of flexible carbon-fibre implants as tendon and ligament substitutes in clinical practice. A preliminary report. *J Bone Joint Surg Br.* **1980**, *62-B* (4), 497–499.

(22) Wang, L.; Wan, F.; Xu, Y.; Xie, S.; Zhao, T.; Zhang, F.; Yang, H.; Zhu, J.; Gao, J.; Shi, X.; et al. Hierarchical helical carbon nanotube fibre as a bone-integrating anterior cruciate ligament replacement. *Nat. Nanotechnol.* **2023**, *18* (9), 1085–1093.

(23) Howard, C. B.; Winston, I.; Bell, W.; Mackie, I.; Jenkins, D. H. Late repair of the calcaneal tendon with carbon fibre. *J Bone Joint Surg Br.* **1984**, *66* (2), 206–208.

(24) Xie, X.; Li, D.; Chen, Y.; Shen, Y.; Yu, F.; Wang, W.; Yuan, Z.; Morsi, Y.; Wu, J.; Mo, X. Conjugate Electrospun 3D Gelatin Nanofiber Sponge for Rapid Hemostasis. *Adv. Healthc. Mater.* **2021**, *10* (20), No. e2100918.

(25) Khan, A. U. R.; Huang, K.; Khalaji, M. S.; Yu, F.; Xie, X.; Zhu, T.; Morsi, Y.; Jinzhong, Z.; Mo, X. Multifunctional bioactive core-shell electrospun membrane capable to terminate inflammatory cycle and promote angiogenesis in diabetic wound. *Bioact. Mater.* **2021**, *6* (9), 2783–2800.

(26) Curry, E. J.; Le, T. T.; Das, R.; Ke, K.; Santorella, E. M.; Paul, D.; Chorsi, M. T.; Tran, K. T. M.; Baroody, J.; Borges, E. R.; et al. Biodegradable nanofiber-based piezoelectric transducer. *Proc. Natl. Acad. Sci. U. S. A.* **2020**, *117* (1), 214–220.

(27) Liu, Y.; Dzidotor, G.; Le, T. T.; Vinikoor, T.; Morgan, K.; Curry, E. J.; Das, R.; McClinton, A.; Eisenberg, E.; Apuzzo, L. N.; et al. Exercise-induced piezoelectric stimulation for cartilage regeneration in rabbits. *Sci. Transl. Med.* **2022**, *14* (627), No. eabi7282.

(28) Phamornnak, C.; Han, B.; Spencer, B. F.; Ashton, M. D.; Blanford, C. F.; Hardy, J. G.; Blaker, J. J.; Cartmell, S. H. Instructive electrospun silk fibroin-based biomaterials for peripheral nerve tissue engineering. *Biomater. Adv.* **2022**, *141*, 213094.

(29) Jiang, S.; Zhao, X.; Chen, S.; Pan, G.; Song, J.; He, N.; Li, F.; Cui, W.; Fan, C. Down-regulating ERK1/2 and SMAD2/3 phosphorylation by physical barrier of celecoxib-loaded electrospun fibrous membranes prevents tendon adhesions. *Biomaterials* **2014**, *35* (37), 9920–9929.

(30) Metz, R.; Verleisdonk, E.-J. M. M.; van der Heijden, G. J.-M.-G.; Clevers, G.-J.; Hammacher, E. R.; Verhofstad, M. H. J.; van der Werken, C. Acute Achilles tendon rupture: minimally invasive surgery versus non operative treatment, with immediate full weight bearing. Design of a randomized controlled trial. *Am J Sports Med.* **2008**, *36* (9), 1688–94.

(31) Chen, J.; Yu, Q.; Wu, B.; Lin, Z.; Pavlos, N. J.; Xu, J.; Ouyang, H.; Wang, A.; Zheng, M. H. Autologous Tenocyte Therapy for Experimental Achilles Tendinopathy in a Rabbit Model. *Tissue Eng. Part A* **2011**, *17* (15–16), 2037–2048.

(32) Brennan, D. A.; Conte, A. A.; Kanski, G.; Turkula, S.; Hu, X.; Kleiner, M. T.; Beachley, V. Mechanical Considerations for Electrospun Nanofibers in Tendon and Ligament Repair. *Adv. Healthcare Mater.* **2018**, *7* (12), No. e1701277.

(33) Minary-Jolandan, M.; Yu, M.-F. Nanoscale characterization of isolated individual type I collagen fibrils: polarization and piezoelectricity. *Nanotechnology* **2009**, *20* (8), 085706.

(34) Zhang, Q.; Zhu, J.; Fei, X.; Zhu, M. A Janus nanofibrous scaffold integrated with exercise-driven electrical stimulation and nanotopological effect enabling the promotion of tendon-to-bone healing. *Nano Today* **2024**, *55*, 102208.

(35) Zhang, J.; Zhang, X.; Wang, C.; Li, F.; Qiao, Z.; Zeng, L.; Wang, Z.; Liu, H.; Ding, J.; Yang, H. Conductive Composite Fiber with Optimized Alignment Guides Neural Regeneration under Electrical Stimulation. *Adv. Healthcare Mater.* **2020**, *10* (3), No. e2000604.

(36) Jalilnejad, N.; Rabiee, M.; Baheiraie, N.; Ghahremanzadeh, R.; Salarian, R.; Rabiee, N.; Akhavan, O.; Zarrintaj, P.; Hejna, A.; Saeb, M. R.; et al. Electrically conductive carbon-based (bio)-nanomaterials for cardiac tissue engineering. *Bioeng. Transl. Med.* **2023**, *8* (1), No. e10347.

(37) Yu, R.; Zhang, H.; Guo, B. Conductive Biomaterials as Bioactive Wound Dressing for Wound Healing and Skin Tissue Engineering. *Nano-Micro Lett.* **2021**, *14* (1), 1.

(38) Meng, J.; Xiao, B.; Wu, F.; Sun, L.; Li, B.; Guo, W.; Hu, X.; Xu, X.; Wen, T.; Liu, J.; et al. Co-axial fibrous scaffolds integrating with carbon fiber promote cardiac tissue regeneration post myocardial infarction. *Mater. Today Bio.* **2022**, *16*, 100415.

(39) Petersen, R. Carbon Fiber Biocompatibility for Implants. *Fibers* **2016**, *4* (1), 1.

(40) Chua, C. Y. X.; Liu, H.-C.; Di Trani, N.; Susnjari, A.; Ho, J.; Scorrano, G.; Rhudy, J.; Sizovs, A.; Lolli, G.; Hernandez, N.; et al. Carbon fiber reinforced polymers for implantable medical devices. *Biomaterials* **2021**, *271*, 120719.

(41) Green, E. C.; Zhang, Y.; Li, H.; Minus, M. L. Gel-spinning of mimetic collagen and collagen/nano-carbon fibers: Understanding multi-scale influences on molecular ordering and fibril alignment. *J. Mech. Behav. Biomed. Mater.* **2017**, *65*, 552–564.

(42) Arambula-Maldonado, R.; Mequanint, K. Carbon-based electrically conductive materials for bone repair and regeneration. *Mater. Adv.* **2022**, *3* (13), 5186–5206.

(43) Yin, H.; Caceres, M. D.; Yan, Z.; Schieker, M.; Nerlich, M.; Docheva, D. Tenomodulin regulates matrix remodeling of mouse tendon stem/progenitor cells in an ex vivo collagen I gel model. *Biochem. Biophys. Res. Commun.* **2019**, *512* (4), 691–697.

(44) Lin, D.; Alberton, P.; Caceres, M. D.; Volkmer, E.; Schieker, M.; Docheva, D. Tenomodulin is essential for prevention of adipocyte accumulation and fibrovascular scar formation during early tendon healing. *Cell Death Dis.* **2017**, *8* (10), No. e3116–e3116.

(45) Al-Qattan, M. M.; Al-Qattan, A. M. Fibromodulin: structure, physiological functions, and an emphasis on its potential clinical applications in various diseases. *J. Coll Physicians Surg Pak.* **2018**, *28* (10), 783–790.

(46) Katoh, M.; Kishimoto, Y.; Ohkawara, B.; Sakai, T.; Ito, M.; Masuda, A.; Ishiguro, N.; Shukunami, C.; Docheva, D.; Ohno, K. Wnt/ $\beta$ -catenin signaling suppresses expressions of Scx, Mxk, and Tnmd in tendon-derived cells. *PLoS One.* **2017**, *12* (7), No. e0182051.

(47) Barrientos, S.; Stojadinovic, O.; Golinko, M. S.; Brem, H.; Tomic-Canic, M. PERSPECTIVE ARTICLE: Growth factors and cytokines in wound healing. *Wound Repair And Regeneration* **2008**, *16* (5), 585–601.

(48) Zheng, Z.; James, A. W.; Li, C.; Jiang, W.; Wang, J. Z.; Chang, G. X.; Lee, K. S.; Chen, F.; Berthiaume, E. A.; Chen, Y.; et al. Fibromodulin reduces scar formation in adult cutaneous wounds by eliciting a fetal-like phenotype. *Signal Transduction Targeted Ther.* **2017**, *2* (1), 17050.